McRae, E. G. (1979). *Rev. Mod. Phys.* **51**, 541–568.
Marten, H. & Meyer-Ehmsen, G. (1985). *Surf. Sci.* **151**, 570–584.
Peng, L. M., Cowley, J. M. & Yao, N. (1988). *Ultramicroscopy*, **26**, 189–194.
Schiff, L. I. (1968). *Quantum Mechanics*. New York: McGraw-Hill.
Tanaka, M., Saito, R., Ueno, K. & Harada, Y. (1980). *J. Electron Microsc.* **20**, 408–412.
Yao, N. & Cowley, J. M. (1989). *Ultramicroscopy*, **31**, 149–157.

Acta Cryst. (1994). A**50**, 366–375

Projection Description of Cubic Quasiperiodic Crystals with Phason Strains*

By Renhui Wang† and Changsong Qin

Department of Physics, Wuhan University, 430072 *Wuhan, People's Republic of China, and Beijing Laboratory of Electron Microscopy, Chinese Academy of Sciences, PO Box* 2724, 100080 *Beijing, People's Republic of China*

Ganghua Lu

Department of Physics, Wuhan University, 430072 *Wuhan, People's Republic of China, Beijing Laboratory of Electron Microscopy, Chinese Academy of Sciences, PO Box* 2724, 100080 *Beijing, People's Republic of China, and Laboratory of Atomic Imaging of Solids, Institute of Metal Research, Chinese Academy of Sciences*, 110015 *Shenyang, People's Republic of China*

Yongchang Feng

Beijing Laboratory of Electron Microscopy, Chinese Academy of Sciences, PO Box 2724, 10080 *Beijing, People's Republic of China, and Laboratory of Atomic Imaging of Solids, Institute of Metal Research, Chinese Academy of Sciences*, 110015 *Shenyang, People's Republic of China*

and Shengqiu Xu

Department of Physics, Wuhan University, 430072 *Wuhan, People's Republic of China*

(*Received* 10 *July* 1993; *accepted* 1 *November* 1993)

Abstract

A new projection description for a cubic quasiperiodic crystal (CQC), including a projection matrix, diffraction-intensity calculation and a linear phason matrix, has been proposed. The simulated electron diffraction patterns with appropriate phason parameters agree well with the experimental ones obtained for a rapidly solidified $V_6Ni_{16}Si_7$ alloy. The transition from the CQC to its crystalline approximants is treated using the linear-phason-strain concept.

1. Introduction

Since the discovery of the icosahedral quasicrystal (IQC) in Al–Mn alloys (Shechtman, Blech, Gratias & Cahn, 1984), other quasiperiodic crystal (QCs) have been reported, such as the decagonal (Bendersky, 1985), dodecagonal (Ishimasa, Nissen & Fukano, 1985) and octagonal (Wang, Chen & Kuo, 1987) phases. All these quasiperiodic crystals have noncrystallographic point symmetries and can be described with quasiperiodic (QP) tilings projected from a higher-dimensional periodic lattice. However, it is possible to construct QP tilings of crystallographically permissible orientational symmetries. For example, Baranidharan, Balagurusamy, Srinivasan, Gopal & Sasisekharan (1989) constructed a QP tiling with fourfold symmetry and Kulkarni (1989) generated a two-dimensional (2D) QP structure belonging to the 4*mm* point-symmetry group using a modified strip-projection method. This QP structure was interpreted as a superlattice structure of the face-centred-cubic disordered Ni–Mo alloy.

Recently, Janssen (1992) deduced symmetry operations of all possible two- and three-dimensional QP structures of rank 4, 5 or 6, including both noncrystallographic point symmetries such as five-, eight-, ten- and twelvefold symmetries and crystallographic

* This project is supported by the National Natural Science Foundation of China.
† Author for correspondence.

point symmetries such as two-, three-, four- and sixfold symmetries. Indeed, Feng, Lu & Withers (1989) found an incommensurate structure with cubic point-group symmetry in a rapidly solidified $V_6Ni_{16}Si_7$ alloy and then Feng *et al.* (1990) proposed a projection model of a cubic quasiperiodic crystal (CQC) to describe the experimental electron diffraction patterns (EDPs) found in the rapidly solidified $V_6Ni_{16}Si_7$ alloy.

On the other hand, the concept of linear phason strain (Lubensky, Socolar, Steinhardt, Bancel & Heiney, 1986) has been extensively used to describe some deviations of observed structure and diffraction patterns from idealized QCs. In some alloys, a QC coexists with its crystalline approximants and some intermediate states between them. The linear-phason-strain treatment has been successfully used to describe the transition from idealized QCs through intermediate states to their crystalline approximants in the case of icosahedral (see, for example, Mai, Tao, Zhang & Zeng, 1989), decagonal (see, for example, Zhang & Kuo, 1990) and octagonal (Mai *et al.*, 1989) QCs.

In the present paper, we provide more experimental results observed in the rapidly solidified $V_6Ni_{16}Si_7$ alloy and propose a new projection description for the CQC, including an appropriate projection matrix, diffraction-intensity calculation, linear phason matrix and a method for drawing section-projection diagrams. Then, we use this description of the CQC to calculate the EDPs and to draw the corresponding section-projection diagrams of the CQC with different values of the phason parameter β. The simulated EDPs with appropriate β values agree well with the experimental ones obtained in the rapidly solidified $V_6Ni_{16}Si_7$ alloy. Finally, the transition from the CQC to crystalline approximants is discussed using the linear-phason-strain concept. Compared with the description proposed by Feng *et al.* (1990), the description in the present paper makes use of a more appropriate projection matrix, which allows one to describe correctly both the EDPs and the structure model of the $V_6Ni_{16}Si_7$ CQC. It can also be used to introduce a linear phason strain explicitly and to study the phase transition from pure CQC through CQC with phason strain to the crystalline approximants.

2. Projection description of the cubic quasiperiodic crystal

2.1. *General principles of the projection method*

Many types of quasilattice may be described by projecting a six-dimensional (6D) cubic lattice with basis vectors $\mathbf{e} = [\mathbf{e}_1, \mathbf{e}_2, \ldots, \mathbf{e}_6]$ into three-dimensional (3D) physical space. These basis vectors possess the following metric tensor:

$$\mathbf{G} = \mathbf{e}^T\mathbf{e} = A^2\begin{bmatrix} 1&0&0&0&0&0\\ 0&1&0&0&0&0\\ 0&0&1&0&0&0\\ 0&0&0&1&0&0\\ 0&0&0&0&1&0\\ 0&0&0&0&0&1 \end{bmatrix}, \tag{1}$$

where the superscript T indicates the transpose of the matrix. Equation (1) shows that these basis vectors are orthogonal to each other and their moduli are A. The inverse of the metric $\mathbf{G}$ is

$$\mathbf{G}^{-1} = \frac{1}{A^2}\begin{bmatrix} 1&0&0&0&0&0\\ 0&1&0&0&0&0\\ 0&0&1&0&0&0\\ 0&0&0&1&0&0\\ 0&0&0&0&1&0\\ 0&0&0&0&0&1 \end{bmatrix}, \tag{2}$$

from which we can construct the reciprocal basis vectors $\mathbf{e}^* = [\mathbf{e}_1^*, \mathbf{e}_2^*, \ldots, \mathbf{e}_6^*]$ as follows:

$$\mathbf{e}^{*T} = \mathbf{G}^{-1}\mathbf{e}^T. \tag{3}$$

These reciprocal basis vectors $\mathbf{e}_i^*$ are also orthogonal, with moduli $A^* = 1/A$.

Now, we introduce a reciprocal metric tensor:

$$\mathbf{G}^* = \mathbf{e}^{*T}\mathbf{e}^*. \tag{4}$$

By inserting (3) into (4), one obtains

$$\mathbf{G}^* = (\mathbf{G}^{-1})^T = \mathbf{G}^{-1}. \tag{5}$$

Let the orthogonal and normalized basis set in the parallel (physical) space be $(\mathbf{E}_1, \mathbf{E}_2, \mathbf{E}_3)$ and that in the perpendicular (complementary) space be $(\mathbf{E}_4, \mathbf{E}_5, \mathbf{E}_6)$. Suppose that the relationship between $\mathbf{e}$ and $\mathbf{E} = [\mathbf{E}_1, \mathbf{E}_2, \ldots, \mathbf{E}_6]$ is

$$\mathbf{e}^T = A\mathbf{S}\mathbf{E}^T. \tag{6a}$$

Then, we have

$$\mathbf{e}^{*T} = (1/A)\mathbf{S}\mathbf{E}^T, \tag{6b}$$

where $\mathbf{S} = [\mathbf{S}_l, \mathbf{S}_r]$ is a 6×6 matrix of which the left part $\mathbf{S}_l$ and the right part $\mathbf{S}_r$ are 6×3 matrices.

The 6D basis vectors $\mathbf{e}$ and $\mathbf{e}^*$ may be decomposed into parallel and perpendicular components

$$\begin{aligned} \mathbf{e} &= \mathbf{e}^{\parallel} + \mathbf{e}^{\perp} \\ \mathbf{e}^* &= \mathbf{e}^{*\parallel} + \mathbf{e}^{*\perp} \end{aligned} \tag{7}$$

and have the following expressions:

$$(\mathbf{e}^{\parallel})^T = A[\mathbf{S}_l 0]\mathbf{E}^T \tag{8a}$$

$$(\mathbf{e}^{\perp})^T = A[0\mathbf{S}_r]\mathbf{E}^T \tag{8b}$$

$$(\mathbf{e}^{*\parallel})^T = (1/A)[\mathbf{S}_l 0]\mathbf{E}^T \tag{9a}$$

$$(\mathbf{e}^{*\perp})^T = (1/A)[0\mathbf{S}_r]\mathbf{E}^T. \tag{9b}$$

By inserting (6*a*) into (1), we obtain

$$\mathbf{S}\mathbf{S}^T = \mathbf{I} \tag{10}$$

with $\mathbf{I}$ being a unit matrix. From (6) and (10), we obtain

$$\mathbf{E}^T = (1/A)\mathbf{S}^T\mathbf{e}^T \tag{11a}$$

$$\mathbf{E}^T = A\mathbf{S}^T(\mathbf{e}^*)^T. \tag{11b}$$

Then, by inserting (11*a*) into (8*a*), we obtain an expression for the projection matrix $\mathbf{P}^{\parallel}$:

$$(\mathbf{e}^{\parallel})^T = \mathbf{P}^{\parallel}\mathbf{e}^T \tag{12a}$$

with

$$\mathbf{P}^{\parallel} = \mathbf{S}_l \cdot \mathbf{S}_l^T. \tag{12b}$$

Similarly, we have

$$(\mathbf{e}^{\perp})^T = \mathbf{P}^{\perp}\mathbf{e}^T \tag{12c}$$

with

$$\mathbf{P}^{\perp} = \mathbf{S}_r \cdot \mathbf{S}_r^T \tag{12d}$$

and

$$\mathbf{P}^{\parallel} + \mathbf{P}^{\perp} = \mathbf{I}. \tag{13}$$

A quasilattice is obtained by projecting a subset $L(\mathbf{r}_0^{\perp})$ of the 6D lattice points into the physical (parallel) space. The selection of the subset $L(\mathbf{r}_0^{\perp})$ of the lattice points is accomplished by first constructing a 3D hyperplane $l(\mathbf{r}_0^{\perp})$ parallel to the physical space and intersecting the perpendicular space at the point with the position vector $\mathbf{r}_0^{\perp}$.

$$l(\mathbf{r}_0^{\perp}) = \left\{ (x_1, x_2, \ldots, x_6) \middle| \sum_{i=1}^{6} x_i \mathbf{e}_i^{\perp} = \mathbf{r}_0^{\perp} \right\},$$

where the x_i are the coordinates of a point in 6D space relative to the basis vector $\mathbf{e}_i$. The subset $L(\mathbf{r}_0^{\perp})$ in the 6D lattice is now given by the definition

$$L(\mathbf{r}_0^{\perp}) = \left\{ \sum_{i=1}^{6} \mathrm{Int}(x_i)\mathbf{e}_i \middle| \sum_{i=1}^{6} x_i \mathbf{e}_i^{\perp} = \mathbf{r}_0^{\perp} \right\},$$

where $\mathrm{Int}(x_i)$ denotes the integer part of x_i. These 6D lattice points are just the origin vertices of all 6D hypercubic cells cut by the hyperplane $l(\mathbf{r}_0^{\perp})$. Then, the 3D quasilattice $L^{\parallel}(\mathbf{r}_0^{\perp})$ is obtained by projecting the subset $L(\mathbf{r}_0^{\perp})$:

$$L^{\parallel}(\mathbf{r}_0^{\perp}) = \left\{ \sum_{i=1}^{6} \mathrm{Int}(x_i)\mathbf{e}_i^{\parallel} \middle| \sum_{i=1}^{6} x_i \mathbf{e}_i^{\perp} = \mathbf{r}_0^{\perp} \right\}. \tag{14}$$

2.2. *Projection matrix for a cubic quasiperiodic crystal*

For the CQC, we choose the 6×3 matrix $\mathbf{S}_l$ in (8*a*) as

$$\mathbf{S}_l = \frac{1}{(1+\alpha^2)^{1/2}} \begin{bmatrix} 1 & 0 & 0 \\ 0 & 1 & 0 \\ 0 & 0 & 1 \\ \alpha & 0 & 0 \\ 0 & \alpha & 0 \\ 0 & 0 & \alpha \end{bmatrix}, \tag{15}$$

where $\alpha = 2^{-1/2}$ is an irrational parameter (see § 3). Fig. 1(*a*) shows the relationship between $\mathbf{e}_i^{\parallel}$ and the unit vectors $\mathbf{E}_1$, $\mathbf{E}_2$, $\mathbf{E}_3$ in the parallel space as selected by (15). Inserting (15) into (12*b*), we get the expression for $\mathbf{P}^{\parallel}$ as

$$\mathbf{P}^{\parallel} = \frac{1}{(1+\alpha^2)} \begin{bmatrix} 1 & 0 & 0 & \alpha & 0 & 0 \\ 0 & 1 & 0 & 0 & \alpha & 0 \\ 0 & 0 & 1 & 0 & 0 & \alpha \\ \alpha & 0 & 0 & \alpha^2 & 0 & 0 \\ 0 & \alpha & 0 & 0 & \alpha^2 & 0 \\ 0 & 0 & \alpha & 0 & 0 & \alpha^2 \end{bmatrix}, \tag{16}$$

and that for $\mathbf{P}^{\perp}$ from (13) as

$$\mathbf{P}^{\perp} = \frac{1}{(1+\alpha^2)} \begin{bmatrix} \alpha^2 & 0 & 0 & -\alpha & 0 & 0 \\ 0 & \alpha^2 & 0 & 0 & -\alpha & 0 \\ 0 & 0 & \alpha^2 & 0 & 0 & -\alpha \\ -\alpha & 0 & 0 & 1 & 0 & 0 \\ 0 & -\alpha & 0 & 0 & 1 & 0 \\ 0 & 0 & -\alpha & 0 & 0 & 1 \end{bmatrix}. \tag{17}$$

According to (17) and (12*c*), we can select $\mathbf{e}_i^{\perp}$ as follows:

$$(\mathbf{e}^{\perp})^T = A\mathbf{S}_r\mathbf{e}^T \tag{8b}$$

with

$$\mathbf{S}_r = \frac{1}{(1+\alpha^2)^{1/2}} \begin{bmatrix} \alpha & 0 & 0 \\ 0 & \alpha & 0 \\ 0 & 0 & \alpha \\ -1 & 0 & 0 \\ 0 & -1 & 0 \\ 0 & 0 & -1 \end{bmatrix}, \tag{18}$$

which is shown in Fig. 1(*b*).

2.3. *Coordinate transformation and zone relation of quasiperiodic crystals*

A 6D reciprocal vector $\mathbf{g}$ may be expressed as

$$\mathbf{g} = \mathbf{n}^*\mathbf{e}^{*T} \tag{19a}$$

with

$$\mathbf{n}^* = [\mathbf{n}_1{}^*\mathbf{n}_2{}^* \ldots \mathbf{n}_6{}^*]$$

being the 6D indices of $\mathbf{g}$ or

$$\mathbf{g} = \mathbf{g}^{\parallel} + \mathbf{g}^{\perp} \tag{19b}$$

with

$$\mathbf{g}^{\parallel} = (g_1{}^{\parallel} g_2{}^{\parallel} g_3{}^{\parallel}) \begin{bmatrix} E_1 \\ E_2 \\ E_3 \end{bmatrix} \tag{19c}$$

and

$$\mathbf{g}^{\perp} = (g_1{}^{\perp} g_2{}^{\perp} g_3{}^{\perp}) \begin{bmatrix} E_4 \\ E_5 \\ E_6 \end{bmatrix} \tag{19d}$$

being, respectively, the components in physical and complementary spaces of the 6D vector $\mathbf{g}$. Noticing that the relationship between different components of a reciprocal vector is the same as that between the corresponding basis vectors, we get the expressions from (11*a*) for the components of $\mathbf{g}^{\parallel}$ and $\mathbf{g}^{\perp}$ as follows:

$$\begin{bmatrix} g_1{}^{\parallel} \\ g_2{}^{\parallel} \\ g_3{}^{\parallel} \end{bmatrix} = A^*\mathbf{S}_i^T(\mathbf{n}^*)^T \tag{20}$$

and

$$\begin{bmatrix} g_1{}^{\perp} \\ g_2{}^{\perp} \\ g_3{}^{\perp} \end{bmatrix} = A^*\mathbf{S}_r^T(\mathbf{n}^*)^T. \tag{21}$$

Similarly, the components of a 6D lattice vector

$$\mathbf{R} = \mathbf{n}\mathbf{e}^T = \mathbf{R}^{\parallel} + \mathbf{R}^{\perp}$$

$$= [R_1{}^{\parallel} R_2{}^{\parallel} R_3{}^{\parallel}] \begin{bmatrix} E_1 \\ E_2 \\ E_3 \end{bmatrix} + [R_1{}^{\perp} R_2{}^{\perp} R_3{}^{\perp}] \begin{bmatrix} E_4 \\ E_5 \\ E_6 \end{bmatrix} \tag{22}$$

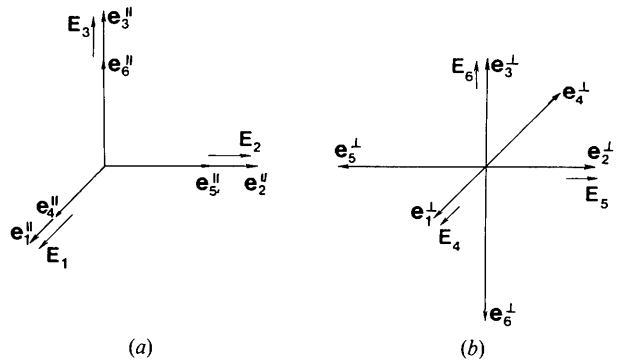

(*a*) (*b*)

Fig. 1. Basis vectors (*a*) $\mathbf{e}_i^{\parallel}$ and (*b*) $\mathbf{e}_i{}^{\perp}$ of the CQC.

have the following expressions:

$$\begin{bmatrix} R_1{}^{\parallel} \\ R_2{}^{\parallel} \\ R_3{}^{\parallel} \end{bmatrix} = A\mathbf{S}_i^T\mathbf{n}^T \tag{23}$$

and

$$\begin{bmatrix} R_1{}^{\perp} \\ R_2{}^{\perp} \\ R_3{}^{\perp} \end{bmatrix} = A\mathbf{S}_r^T\mathbf{n}^T \tag{24}$$

with

$$\mathbf{n} = [n_1 n_2 \ldots n_6]$$

being the 6D indices of $\mathbf{R}$ relative to the basis vectors $\mathbf{e}_i$.

In the case of crystals, the zone relation

$$\mathbf{R} \cdot \mathbf{g} = 0 \tag{25a}$$

is expressed as

$$[u\,v\,w] \begin{bmatrix} h \\ k \\ l \end{bmatrix} = 0, \tag{25b}$$

where $[uvw]$ are the indices of the zone axis $\mathbf{R}$ and $[hkl]$ are the indices of reciprocal vectors $\mathbf{g}$ belonging to the zone axis $\mathbf{R}$. In the case of quasiperiodic crystals, the zone relation

$$\mathbf{R}^{\parallel} \cdot \mathbf{g}^{\parallel} = 0 \tag{25c}$$

can be obtained from (20), (23) and (12*b*) to be

$$\mathbf{n}\mathbf{P}^{\parallel}\mathbf{n}^{*T} = 0. \tag{25d}$$

2.4. *Diffraction-intensity calculation for the cubic quasiperiodic crystal*

In the present work, we apply the same method to calculate the diffraction intensities of the CQC as that used by Zhao, Wang, Cheng & Wang (1988) for icosahedral QC. For simplicity, we have considered only the simple lattice model, in which the same atoms, with unit atomic scattering factor $f(\mathbf{g}^{\parallel}) = 1$, are placed at every quasilattice point. The special characteristics of the CQC compared with the icosahedral QC are that the tiles of the CQC are tetragonal prisms (including cubes) instead of rhombohedra and that there are only eight types of tetragonal prisms with nonzero volume. We denote $v_{ijk} = |\mathbf{e}_i^{\parallel} \times \mathbf{e}_j^{\parallel} \cdot \mathbf{e}_k^{\parallel}|A^3$ as the volume of the tetragonal prism projected from the hypersurface with edges $\mathbf{e}_i$, $\mathbf{e}_j$ and $\mathbf{e}_k$ in the 6D space into the parallel space and $v_{lmn} = |\mathbf{e}_l{}^{\perp} \times \mathbf{e}_m{}^{\perp} \cdot \mathbf{e}_n{}^{\perp}|A^3$ as that from the $\mathbf{e}_l$, $\mathbf{e}_m$ and $\mathbf{e}_n$ hypersurface into the perpendicular space, where l, m and n are the complementary indices of i, j and k:

$$\{l, m, n\} = \{1, 2, \ldots, 6\} - \{i, j, k\}.$$

From (8), (15) and (18), it is obvious that $v_{ijk} = v_{lmn}$. Table 1 lists the triplets (i, j, k) and the corresponding volumes $v_{ijk} = v_{lmn}$ of the CQC. In the case of a CQC, the fraction w_n of the nth atom belonging to a tetragonal prism is equal to 1/8. Noticing these special characterists of the CQC and following the line described by Zhao *et al.* (1988), we obtain the scattering amplitude $S(\mathbf{g}^{\parallel})$ per atom as follows:

$$S(\mathbf{g}^{\parallel}) = (1/\mu) \sum_{i,j,k} V_{lmn}[\sin(z_l)/z_l][\sin(z_m)/z_m] \times [\sin(z_n)/z_n]\cos(z_i)\cos(z_j)\cos(z_k), \quad (26)$$

where $\mu = [(1+\alpha)/(1+\alpha^2)^{1/2}]^3 A^3$ is the projected volume of a 6D hypercube and is equal to the sum of the v_{lmn} that are listed in Table 1. The factor z_α in (26) is defined as

$$z_\alpha = \pi \mathbf{g}^{\perp} \cdot \mathbf{e}_\alpha{}^{\perp}$$

and the summation in (26) is over eight sets of i, j, k as listed in Table 1.

2.5. *Phason strains in the cubic quasiperiodic crystal*

A CQC may not be ideal but, with a phason strain field,

$$\Delta\mathbf{r}^{\perp}(\mathbf{r}^{\parallel}) = [\Delta r_1{}^{\perp}, \Delta r_2{}^{\perp}, \Delta r_3{}^{\perp}] \begin{bmatrix} \mathbf{E}_4 \\ \mathbf{E}_5 \\ \mathbf{E}_6 \end{bmatrix}.$$

Over a given small region of the CQC, the phason strain field may be described approximately as a linear function of the position vector

$$\mathbf{r}^{\parallel} = [r_1{}^{\parallel}, r_2{}^{\parallel}, r_3{}^{\parallel}] \begin{bmatrix} \mathbf{E}_1 \\ \mathbf{E}_2 \\ \mathbf{E}_3 \end{bmatrix},$$

i.e.:

$$[\Delta r_1{}^{\perp}\ \Delta r_2{}^{\perp}\ \Delta r_3{}^{\perp}] = [r_1{}^{\parallel} r_2{}^{\parallel} r_3{}^{\parallel}]\mathbf{X}, \quad (27a)$$

with $\mathbf{X}$ being a 3×3 phason matrix. For a special case when

$$\mathbf{X} = -\begin{bmatrix} \beta & 0 & 0 \\ 0 & \beta & 0 \\ 0 & 0 & \beta \end{bmatrix}, \quad (27b)$$

the symmetry of the CQC with phason strain remains cubic. According to Lubensky *et al.* (1986), a linear phason strain will cause each Bragg peak to shift from the position pointed to by the reciprocal vector $\mathbf{g}^{\parallel}$ of an unstrained CQC to $\mathbf{g}^{\parallel\prime} = \mathbf{g}^{\parallel} + \Delta\mathbf{g}^{\parallel}$ with

$$\begin{bmatrix} \Delta g_1{}^{\parallel} \\ \Delta g_2{}^{\parallel} \\ \Delta g_3{}^{\parallel} \end{bmatrix} = -\mathbf{X} \begin{bmatrix} g_1{}^{\perp} \\ g_2{}^{\perp} \\ g_3{}^{\perp} \end{bmatrix},$$

Table 1. *Triplets (i, j, k) and corresponding volumes $v_{ijk} = v_{lmn}$ of the CQC*

Triplet i, j, k	V_{ijk}/A^3
1, 2, 3	$(1+\alpha^2)^{-3/2}$
1, 2, 6	$\alpha(1+\alpha^2)^{-3/2}$
1, 3, 5	$\alpha(1+\alpha^2)^{-3/2}$
1, 5, 6	$\alpha^2(1+\alpha^2)^{-3/2}$
2, 3, 4	$\alpha(1+\alpha^2)^{-3/2}$
2, 4, 6	$\alpha^2(1+\alpha^2)^{-3/2}$
3, 4, 5	$\alpha^2(1+\alpha^2)^{-3/2}$
4, 5, 6	$\alpha^3(1+\alpha^2)^{-3/2}$

the corresponding perpendicular components $\mathbf{g}^{\perp}$ being kept unchanged. By using (20) and (21), we obtain

$$\begin{bmatrix} g_1{}^{\parallel\prime} \\ g_2{}^{\parallel\prime} \\ g_3{}^{\parallel\prime} \end{bmatrix} = \frac{A^*}{(1+\alpha^2)^{1/2}} \begin{bmatrix} (1+\alpha\beta)n_1{}^* + (\alpha-\beta)n_4{}^* \\ (1+\alpha\beta)n_2{}^* + (\alpha-\beta)n_5{}^* \\ (1+\alpha\beta)n_3{}^* + (\alpha-\beta)n_6{}^* \end{bmatrix}. \quad (28)$$

2.6. *Section-projection diagrams of quasicrystalline tilings*

The structure of a quasicrystalline tiling with phason and phonon strains can be described visually by a section-projection diagram (Katz & Duneau, 1986), which is drawn by cutting the tiling along a given quasilattice plane P and projecting the corresponding 2D boundary surfaces into P. If the distance of a plane P from the origin along the direction $\mathbf{D}$ in the parallel space is d, then the quasilattice point set $P(\mathbf{r}_0{}^{\perp}, d)$ on the 2D boundary surface of the plane P can be extracted from (14) to be

$$P(\mathbf{r}_0{}^{\perp}, d) = \left\{ \sum_{i=1}^{6} \mathrm{Int}(x_i)\mathbf{e}_i{}^{\parallel} \,\middle|\, \sum_{i=1}^{6} x_i \mathbf{e}_i{}^{\perp} = \mathbf{r}_0{}^{\perp} \text{ and } \mathbf{D} \cdot \sum_{i=1}^{6} x_i \mathbf{e}_i{}^{\parallel} = d \right\}. \quad (29)$$

From the 6D coordinates $\mathrm{Int}(x_i)$ relative to the basis set $\mathbf{e}_i$ and using the coordinate transformation (23), we obtain the coordinates $r_i{}^{\parallel}$ $(i = 1, 2, 3)$ of the quasilattice points surrounding the plane P relative to the basis set $\mathbf{E}_i$ $(i = 1, 2, 3)$ in 3D physical space. The section-projection diagram is now obtained by projecting these points orthogonally onto the plane P and connecting each pair of projected points that are neighbouring lattice points in the 6D space.

A section-projection diagram of the QC with phason strain $\Delta\mathbf{r}^{\perp}$ and/or phonon strain $\Delta\mathbf{r}^{\parallel}$ is obtained by replacing $\mathbf{r}_0{}^{\perp}$ in (29) by $\mathbf{r}_0{}^{\perp} - \Delta\mathbf{r}^{\perp}$ and adding the displacement $\Delta\mathbf{r}^{\parallel}$ to each position vector $\mathbf{r}^{\parallel}$ of the quasilattice point surrounding the plane P.

Table 2. *Sequence numbers, indices* n_1^*, n_2^*, ..., n_6^* *and calculated intensities* I/I_0 *of reflections of the CQC*

Spot	n_1^*	n_2^*	n_3^*	n_4^*	n_5^*	n_6^*	I/I_0
0	0	0	0	0	0	0	1.000
1	0	1	1	0	0	0	0.717
2	0	2	2	0	0	0	0.264
3	0	1	1	0	2	2	0.326
4	0	2	2	0	2	2	0.796
5	0	3	3	0	2	2	0.990
6	2	0	0	0	0	0	0.514
7	4	0	0	4	0	0	0.633
8	6	0	0	4	0	0	0.981
9	0	0	0	1	1	1	0.369
10	0	1	1	1	1	1	0.677
11	0	2	2	1	1	1	0.639
12	2	0	0	2	0	0	0.892
13	2	1	1	1	1	1	0.892
14	2	2	2	1	1	1	0.843
15	2	3	3	1	3	3	0.564
16	2	1	1	2	0	0	0.639
17	2	2	2	2	2	2	0.709
18	2	3	3	2	2	2	0.884
19	4	0	0	2	0	0	0.796
20	4	1	1	3	1	1	0.935
21	4	2	2	3	1	1	0.883
22	4	3	3	3	3	3	0.592
23	1	1	2	0	0	0	0.343
24	1	1	2	0	2	2	0.339

3. Experimental and simulation methods

Pure vanadium, nickel and silicon were melted into an alloy of nominal composition $V_6Ni_{16}Si_7$ and then rapidly quenched. Transmission electron microscope (TEM) specimens were prepared by ion-milling and were examined with EM420 and EM430 electron microscopes. The experimental detail was as described by Feng *et al.* (1987).

The simulation procedure of an EDP of the zone axis $\mathbf{R}^{\parallel}$ is as follows: all the 6D reciprocal-lattice vectors $\mathbf{g}(n_1^*, ..., n_6^*)$ with $-4 \le n_i^* \le 4$ are selected in turn and their corresponding 3D vectors $\mathbf{g}^{\parallel\prime}(n_1^*, ..., n_6^*)$ with a phason parameter β are calculated according to (28). Then, we only consider reflections $\mathbf{g}^{\parallel}$ satisfying the zone relation (25*c*) and calculate their diffraction amplitude $S(\mathbf{g}^{\parallel})$ according to (26). Since the scattering amplitude $S(\mathbf{g}^{\parallel})$ depends mainly on the perpendicular component $\mathbf{g}^{\perp}$, which remains unchanged when the phason parameter β is varied, we can assume that the diffraction intensity is independent of β. For this reason, we first tried a series of α values. By comparing the simulated EDPs with the experimental ones, we found good agreement in diffraction intensities if we took the α value to be 0.68–0.72 and the following reflection condition:

$$\begin{aligned} n_1^* + n_2^* + n_3^* &= 2m_1 \\ n_5^* + n_6^* &= \begin{cases} 2m_2 \\ 4m_2 \end{cases} \quad \text{when } n_4^* = 0 \\ n_6^* + n_4^* &= \begin{cases} 2m_3 \\ 4m_3 \end{cases} \quad \text{when } n_5^* = 0 \\ n_4^* + n_5^* &= \begin{cases} 2m_4 \\ 4m_4 \end{cases} \quad \text{when } n_6^* = 0 \end{aligned} \tag{30}$$

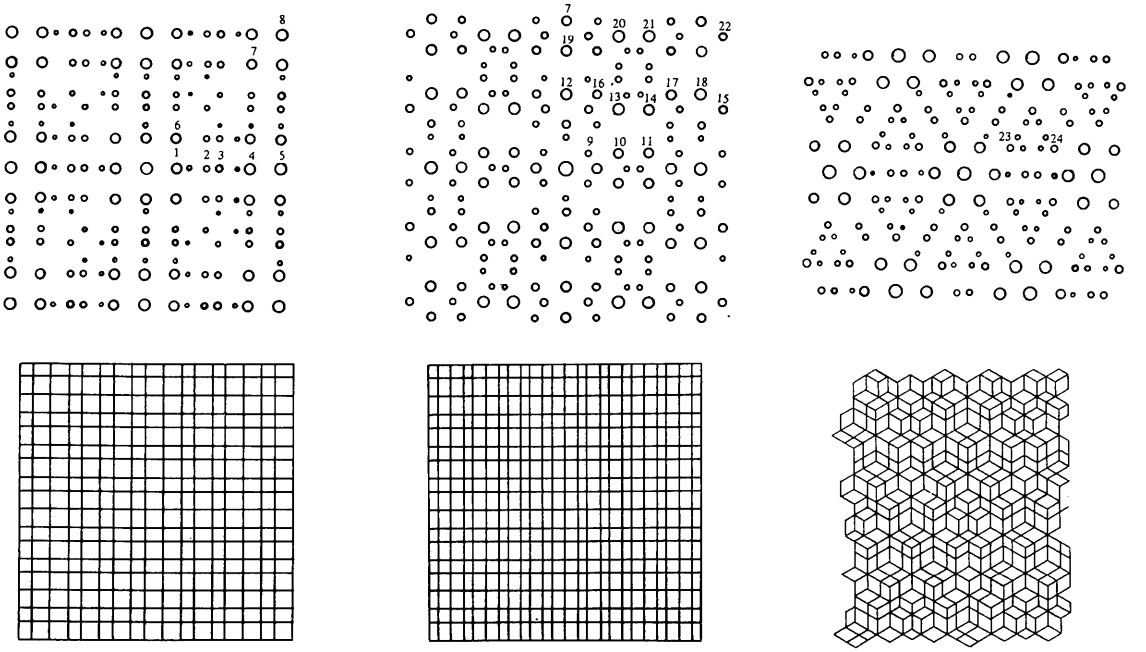

Fig. 2. Simulated EDPs (top) and section-projection diagrams (bottom) perpendicular to the [100] (left), [01$\bar{1}$] (middle) and [11$\bar{1}$] (right) zone axes of the CQC. The length of the scale bar is equal to $a = A/(1 + \alpha^2)^{1/2}$.

with the m_i being integers. Then, we fixed α at $2^{-1/2}$ and varied β to obtain good agreement in reflection intensities as well as positions.

In some cases, the section-projection diagrams perpendicular to the zone axes [100], [01$\bar{1}$] and [11$\bar{1}$] were drawn to describe visually the features of the CQC tilings with various phason strains.

4. Results

Fig. 2 shows the simulated EDPs (top) and corresponding section-projection diagrams (bottom) perpendicular to the [100] (left), [01$\bar{1}$] (middle) and [11$\bar{1}$] (right) zone axes when $\alpha = 2^{-1/2}$ and $\beta = 0$. The sequence numbers marked at the reflection spots, their 6D indices n_1*, ..., n_6* and calculated intensities I/I_0 are listed in Table 2. In the present paper, the size of each circle of a simulated EDP is proportional to the reflection intensity. In the simulated twofold-axis EDPs, we also marked the spots 12, 16 and 19, which are extinct according to (30) but can appear by multiple reflection. The distribution of reflections shows an aperiodic feature with cubic point symmetry but there is no apparent periodic main-reflection lattice consisting of strong diffraction peaks surrounded by weak satellite peaks. Therefore, it is not appropriate to attribute it to a cubic incommensurate crystal and we use the term 'cubic quasiperiodic crystal' (CQC) instead. The section-projection diagrams reveal that the so-called CQC tiling consists of large and small cubes of edges of $A/(1+\alpha^2)^{1/2}$ and $\alpha A/(1+\alpha^2)^{1/2}$, respectively, and tetragonal prisms with these edges. Their distribution shows aperiodic features and the number ratio of the large and small cubes is $1{:}\alpha^3 = 1{:}0.35$.

The relative reflection intensities of all our photographed EDPs are in good agreement with Fig. 2. Nevertheless, the reflection-position distribution in an EDP may change when the observed area is changed and we have not yet observed an EDP that possesses the same reflection-position distribution as in Fig. 2. This fact indicates that we have not yet observed experimentally a perfect CQC. One set of experimental EDPs is shown in the upper part of Fig. 3. The main feature of these EDPs is the same as that of Fig. 2 but the reflection distribution is different. By choosing the 6D lattice constant $A = 1.07$ nm and an appropriate phason parameter $\beta = 0.303$, we obtain good agreement between the experimental (top) and simulated (bottom) EDPs as shown in Fig. 3.

In general, EDPs of a given [100], [01$\bar{1}$] or [11$\bar{1}$] zone axis from different regions of the rapidly solidified $V_6Ni_{16}Si_7$ alloy have the same main features but different reflection distributions corresponding to different phason strains. For example, Fig. 4 shows a

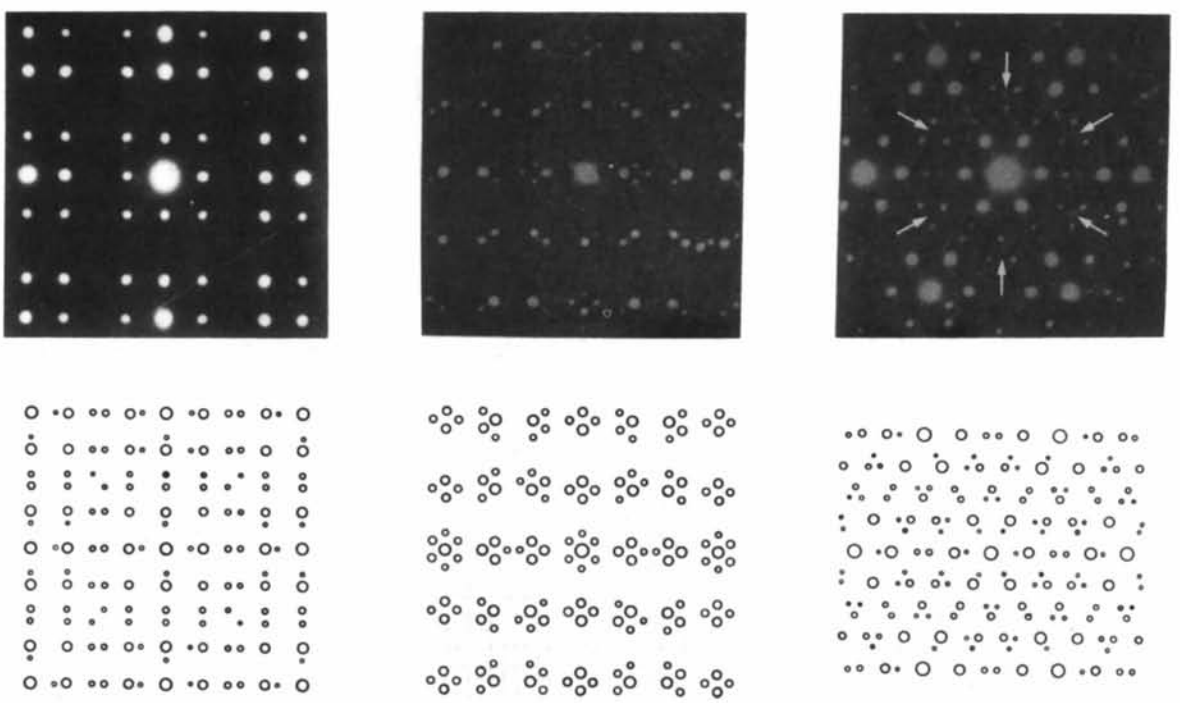

Fig. 3. Experimental (top) and simulated (bottom) [100] (left), [01$\bar{1}$] (middle) and [11$\bar{1}$] (right) zone-axis EDPs of a rapidly quenched $V_6Ni_{16}Si_7$ alloy.

series of [100] zone-axis EDPs from different regions of the alloy. By choosing different appropriate values of the phason parameter β, we succeeded in simulating these EDPs as shown in Fig. 5 with (*a*) $\beta = 0.303$, (*b*) $\beta = 0.443$, (*c*) $\beta = 0.588$ and (*d*) $\beta = 0.707$. The corresponding section-projection diagrams are shown in Fig. 6.

From Figs. 2, 4 and 5, it is obvious that with the increase of the β parameter the separation between reflections 1 and 3 decreases and they converge into a single spot when $\beta = 0.707$. The same situation holds for reflections 2 and 4. However, the shift of reflection 5 is negligible. Fig. 4 reveals also that the variation of the reflection intensities is negligible when the parameter β is changed as we assumed in § 3.

Fig. 6 shows that the cubic quasiperiodic lattice with phason strain consists of cubes and tetragonal prisms. The relative number of small cubes decreases with increasing β and the CQC becomes a cubic crystal consisting only of large cubes when $\beta = 0.707$. Its EDP (Figs. 4*d* and 5*d*) resembles that of a body-centred-cubic (b.c.c.) crystal, *e.g.* the alloy phase of α-Mn or γ-brass structure, with lattice constant $a \simeq 0.88$ nm.

5. Discussion

Substituting the indices $n_1^*, \ldots, n_6^*$ of the reflections 1, 2, 3, 4 and 5 shown in Fig. 2 into (28), we obtain the expression for the magnitudes of these reciprocal vectors as follows:

$$g^{\parallel\prime} = K[(n_2^* + \alpha n_5^*) + (n_2^*\alpha - n_5^*)\beta]$$

with

$$K = 2^{1/2}A^*/(1 + \alpha^2)^{1/2};$$

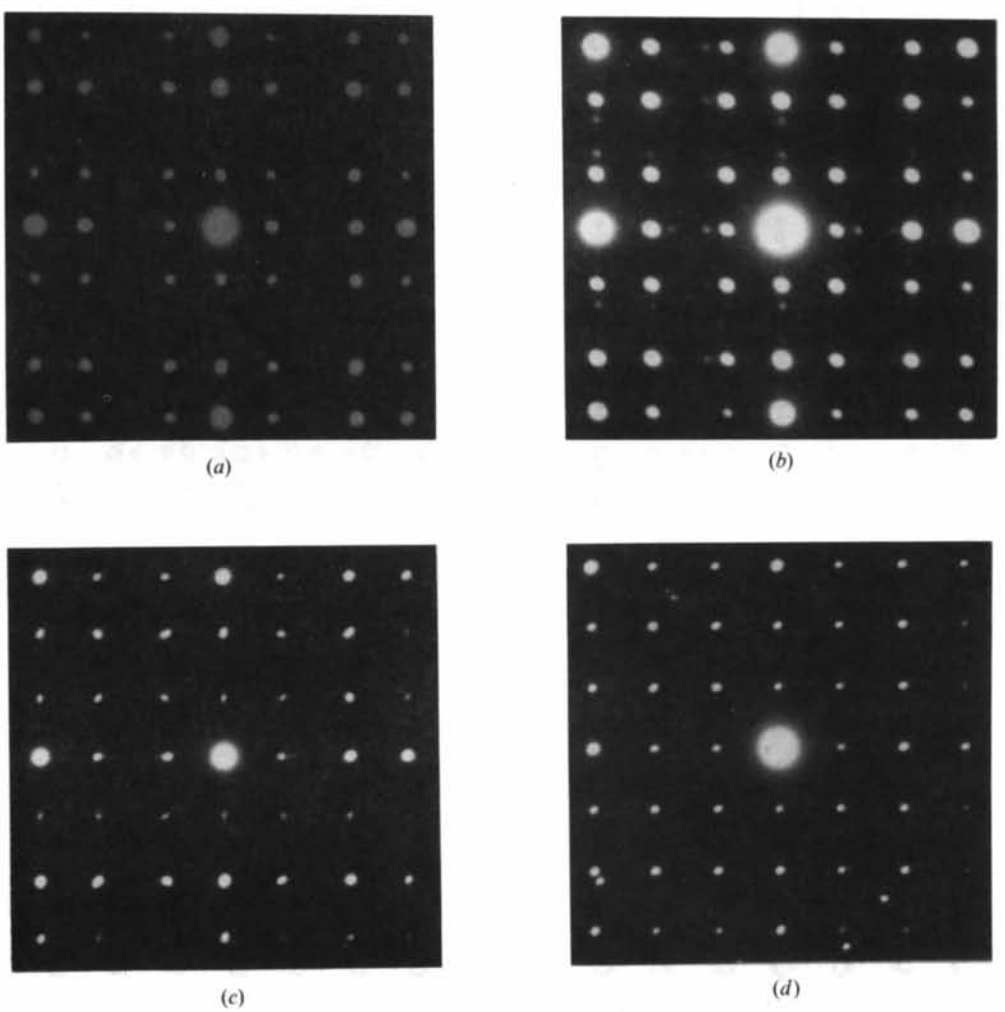

Fig. 4. [100]-zone-axis EDPs from different regions of the rapidly solidified $V_6Ni_{16}Si_7$ alloy.

hence, we have

$$g^{\parallel\prime}(1) = K(1 + 0.707\beta)$$
$$g^{\parallel\prime}(2) = K(2 + 1.414\beta)$$
$$g^{\parallel\prime}(3) = K(2.414 - 1.293\beta)$$
$$g^{\parallel\prime}(4) = K(3.414 + 0.586\beta)$$
$$g^{\parallel\prime}(5) = K(4.414 + 0.121\beta).$$

From these expressions, it is apparent that, with the increase of the β parameter, $g^{\parallel\prime}(3)$ and $g^{\parallel\prime}(4)$ decrease and $g^{\parallel\prime}(1)$, $g^{\parallel\prime}(2)$ and $g^{\parallel\prime}(5)$ increase. But the increment of $g^{\parallel\prime}(5)$ is very small, less than 2% when β increases from 0 to 0.707. This is in good agreement with the observation described in § 4.

When $1 + \alpha\beta = mc$ and $\alpha - \beta = nc$ (m and n are integers without any common divisor except 1), (28) becomes

$$\begin{bmatrix} g_1^{\parallel\prime} \\ g_2^{\parallel\prime} \\ g_3^{\parallel\prime} \end{bmatrix} = \frac{cA^*}{(1+\alpha^2)^{1/2}} \begin{bmatrix} mn_1^* + nn_4^* \\ mn_2^* + nn_5^* \\ mn_3^* + nn_6^* \end{bmatrix}.$$

Table 3. *Phason parameters β and the lattice types and lattice parameters a of the corresponding crystalline approximants*

β	m	n	c	a (Å)	Lattice type
$-2^{1/2}$	0	1	2.121	6.2	f.c.c.
−0.536	1	2	0.621	21.1	b.c.c.
0.153	2	1	0.554	23.7	f.c.c.
0.707	1	0	1.5	8.7	b.c.c.

and hence all the $g^{\parallel\prime}$ become reciprocal vectors of a cubic crystal of lattice constant $a = (1 + \alpha^2)^{1/2}A/c$. Some possible crystalline approximants of the CQC are listed in Table 3. From the values m and n and the reflection condition (30), we can also obtain the reflection condition for $g^{\parallel\prime}$ and hence the lattice type of each approximant. The b.c.c. approximant with $\beta = 0.707$ is exactly the one shown in Fig. 4(*d*). The face-centred cubic (f.c.c.) approximant with $\beta = 0.153$ was observed by Feng *et al.* (1990) and occurs when reflections 2 and 3 converge into one single spot.

In the present work, we have calculated the diffraction intensities by a simplified kinematical

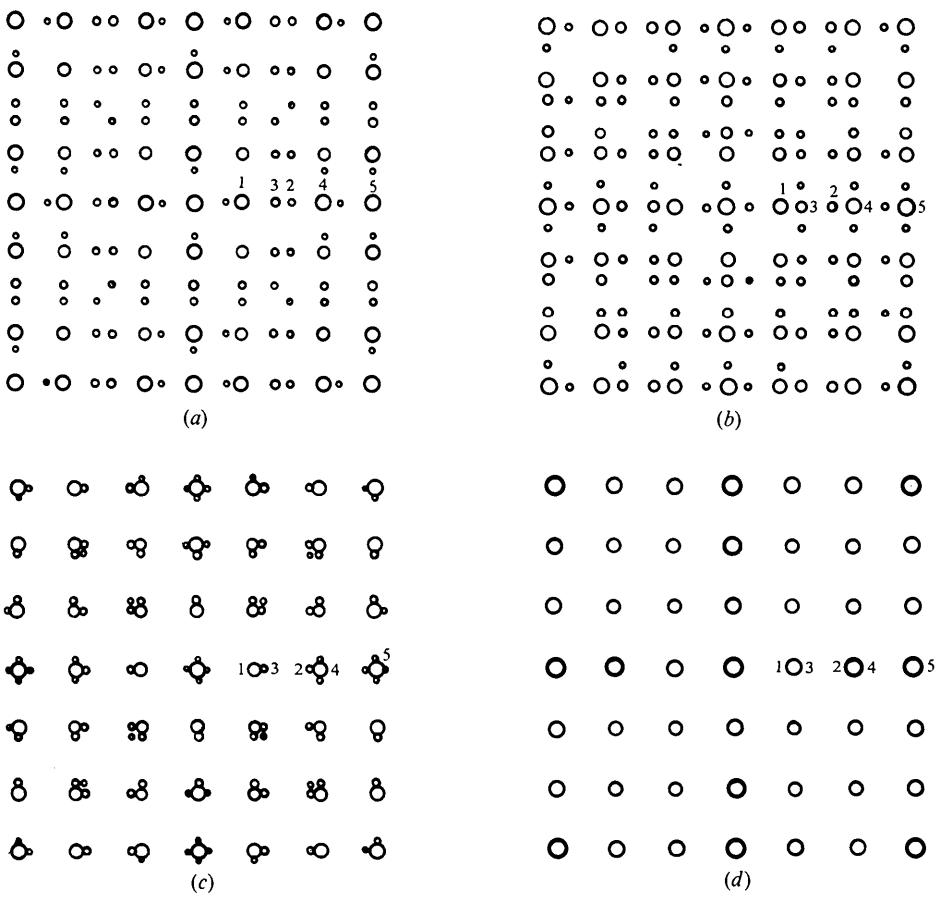

Fig. 5. Simulated [100] zone-axis EDPs of the CQC. β = (*a*) 0.303, (*b*) 0.443, (*c*) 0.588 and (*d*) 0.707.

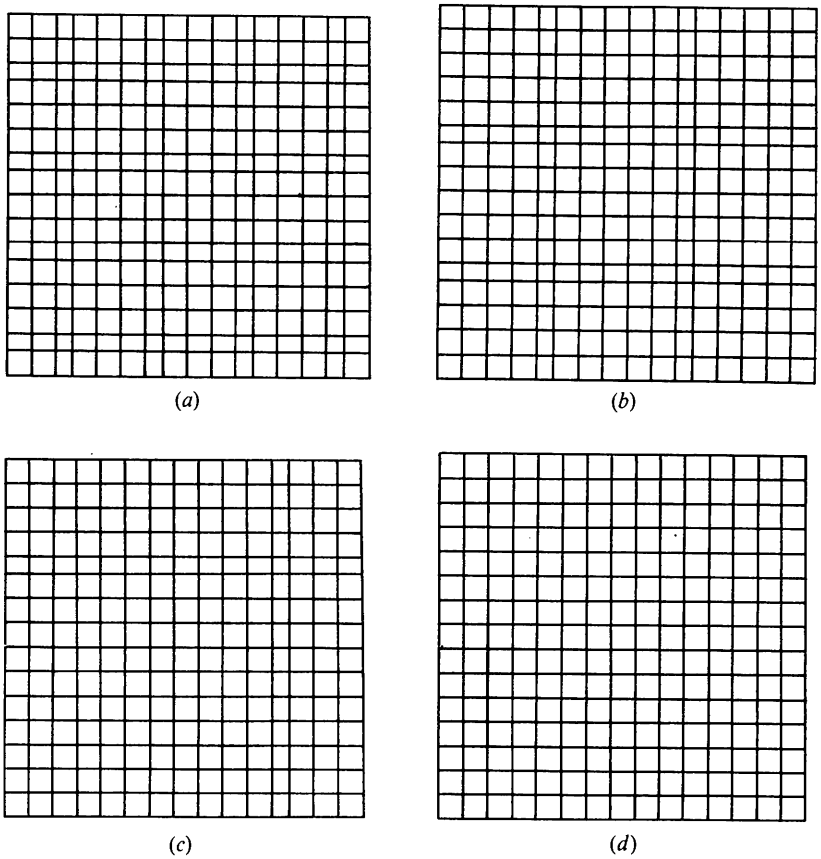

Fig. 6. Section-projection diagrams of the CQC perpendicular to the [100] zone axis. β = (*a*) 0.303, (*b*) 0.443, (*c*) 0.588 and (*d*) 0.707.

approximation and a simple lattice model, which may be the reason that there exist some minor discrepancies between the experimental and simulated EDPs. Moreover, the reciprocal points of any QP structure are generally distributed very densely. Hence, there may be some reciprocal points that contribute to the [*uvw*] zone axis EDP, although they do not belong to this zone axis, lying somewhat above or below the (*uvw*)* reciprocal plane through the origin. On the other hand, in a simulated [*uvw*] zone axis EDP, we choose only those points that belong exactly to this zone axis according to (25*c*). For example, the weak spots arrowed in the experimental [11$\bar{1}$] zone axis EDP in Fig. 3 were not simulated because they are from the reciprocal points lying somewhat above the (11$\bar{1}$)* reciprocal plane. For a detailed discussion of this effect, see Feng *et al.* (1990).

References

Baranidharan, S., Balagurusamy, V. S. K., Srinivasan, A., Gopal, E. S. R. & Sasisekharan, V. (1989). *Phase Transit.* **16/17**, 621–626.

Bendersky, L. (1985). *Phys. Rev. Lett.* **55**, 1461–1463.

Feng, Y. C., Lu, G. & Withers, R. L. (1989). *J. Phys. Condens. Matter*, **1**, 3695–3700.

Feng, Y. C., Lu, G., Ye, H. Q., Kuo, K. H., Withers, R. L. & Van Tendeloo, G. (1990). *J. Phys. Condens. Matter*, **2**, 9749–9755.

Feng, Y. C., Zhou, D. S., Li, D. X., Dong, C., Van Tendeloo, G. & Kuo, K. H. (1987). *Philos. Mag. Lett.* **55**, 221–224.

Ishimasa, T., Nissen, H.-U. & Fukano, Y. (1985). *Phys. Rev. Lett.* **55**, 511–513.

Janssen, T. (1992). *Z. Kristallogr.* **198**, 17–32.

Katz, A. & Duneau, M. (1986). *J. Phys. (Paris)*, **47**, 181–196.

Kulkarni, U. D. (1989). *Phys. Rev. Lett.* **63**, 2484–2487.

Lubensky, T. C., Socolar, J. E. S., Steinhardt, P. J., Bancel, P. A. & Heiney, P. A. (1986). *Phys. Rev. Lett.* **57**, 1440–1443.

Mai, Z. H., Tao, S. Z., Zhang, B. S. & Zeng, L. Z. (1989). *J. Phys. Condens. Matter*, **1**, 2465–2471.

Mai, Z. H., Xu, L., Wang, N., Kuo, K. H., Jin, Z. C. & Cheng, G. (1989). *Phys. Rev. B*, **40**, 12183–12186.

Shechtman, D., Blech, I., Gratias, D. & Cahn, J. W. (1984). *Phys. Rev. Lett.* **53**, 1951–1953.

Wang, N., Chen, H. & Kuo, K. H. (1987). *Phys. Rev. Lett.* **59**, 1010–1013.

Zhang, H. & Kuo, K. H. (1990). *Phys. Rev. B*, **42**, 8907–8914.

Zhao, D., Wang, R., Cheng, Y. & Wang, Z. (1988). *J. Phys. F*, **18**, 1893–1904.